ACS APPLIED MATERIALS & INTERFACES

Research Article

www.acsami.org

Dually Fixed SnO_2 Nanoparticles on Graphene Nanosheets by Polyaniline Coating for Superior Lithium Storage

Yanfeng Dong, Zongbin Zhao,* Zhiyu Wang, Yang Liu, Xuzhen Wang, and Jieshan Qiu*

Carbon Research Laboratory, Liaoning Key Lab for Energy Materials and Chemical Engineering, State Key Lab of Fine Chemicals, School of Chemical Engineering, Dalian University of Technology, Dalian 116023, China

Supporting Information

ABSTRACT: Dually fixed SnO_2 nanoparticles (DF-SnO_2 NPs) on graphene nanosheets by a polyaniline (Pani) coating was successfully fabricated via two facile wet chemistry processes, including anchoring SnO_2 NPs onto graphene nanosheets via reducing graphene oxide by Sn^{2+} ion, followed by *in situ* surface sealing with the Pani coating. Such a configuration is very appealing anode materials in LIBs due to several structural merits: (1) it prevents the aggregation of SnO_2 NPs, (2) accommodates the structural expanding of SnO_2 NPs during lithiation, (3) ensures the stable as-formed solid electrolyte interface films, and (4) effectively enhances the electronic conductivity of the overall electrode. Therefore, the final DF-SnO_2 anode exhibits stable cycle performance, such as a high capacity retention of over 90% for 400 cycles at a current density of 200 mA g^{-1} and a long cycle life up to 700 times at a higher current density of 1000 mA g^{-1}.

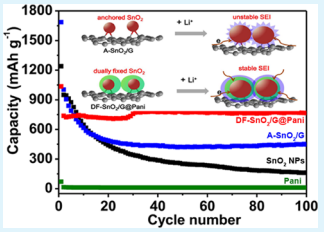

KEYWORDS: *tin dioxide, graphene, polyaniline, phytic acid, Li-ion batteries*

INTRODUCTION

Due to the advantages of high energy density and environmental benignity, lithium-ion batteries (LIBs) are currently the predominant power source for portable electronics and have shown great promise in upcoming large-scale applications.[1−4] The continuously surging demanding emerging large-scale energy applications such as low-emission electric vehicles, renewable power plants, and electric grids boost a great deal of interest in seeking high-performance and long-life electrodes.[2] Tin dioxide (SnO_2) is one of the most extensively studied anode materials for its relative abundance, safe lithiation potential, and high theoretical specific capacity (782 mAh g^{-1}), which is more than twice that of graphite (370 mAh g^{-1}).[5,6] However, SnO_2 suffers from large volume expansion (~250%) during full charge/discharge cycling, resulting in fracture and loss of electrical contact, and an unstable solid electrolyte interphase (SEI) growth on the SnO_2 surface, which has been confirmed by direct real-time visualization of the lithiation of the SnO_2 nanowire inside a transmission electron microscope.[7] Macroscopically, rapid capacity decay and poor cycling stability are obtained.[5,8] Nanostructured SnO_2 could have some positive effect to overcome these shortcomings,[8−10] such as nanosphere,[11,12] nanotubes,[13] nanosheets,[14] and hollow nanostructures;[8] however, few successes were done for a long-life (>300 cycles) pure SnO_2 anode, due to its intrinsic low charge/ionic conductivity and self-aggregation between nanoparticles.[8,15]

Building hybrid nanostructures has been regarded as one of the most effective approaches toward high-performance anode materials for LIBs. Graphene, one-atom-thick two-dimensional layers of sp^2-bonded carbon, shows great potentials for compositing with SnO_2 for LIBs, such as mesoporous SnO_2/graphene,[16] SnO_2 nanorods/graphene,[17] 3D hierarchical SnO_2/graphene frameworks,[18] and N-doped graphene/SnO_2 sandwich paper.[15] In these nanocomposites, the presence of the graphene can effectively buffer the strain caused by structural and volume changes of SnO_2 NPs, prevent them from the aggregation during cycling and form a highly flexible 2D/3D electronic network to facilitate the charge transfer,[18] improve the conductivity of SnO_2, and accommodate the volume expansion upon Li insertion/extraction.[18−20] Unfortunately, most of SnO_2/G electrodes, except for elaborately designed ones,[19,21] usually exhibit unsatisfied capacity and short cycle life (<300 cycles);[18,20,22,23] the reasons are mainly ascribed to unstable SEI films and weak interactions between substrates and SnO_2. A heterogeneous coating is another effective strategy to form stable SEI films and keep the structural integrity; thus, the cycling stability of SnO_2 composites is enhanced.[4,5,24−28] For example, a glucose-derived carbon layer has been coated on SnO_2 hierarchical tubes via a hydrothermal method; in contrast to its counterpart without coating, the final hybrid shows stable cycle ability and higher capacity in 50 cycles. Metal oxide layers have been coated on nanostructured SnO_2 via a hydrothermal reaction and atomic layer deposition method.[4,27,28] Unfortunately, these coating layers are not elastic and cannot intimately interact with active materials, so few of them could withstand repeatedly charge/discharge cycles for a long time.

Notwithstanding these advances, the rational design and controllable synthesis of SnO_2-based electrodes with superior lithium storage performance remain as a great challenge. Two-dimensional graphene nanosheets may have potential to further construct unique nanostructured SnO_2-based hybrids. The ideal nanoarchitecture is embedding SnO_2 NPs into a conductive

Received: October 18, 2014
Accepted: December 31, 2014
Published: December 31, 2014

DOI: 10.1021/am506818h
ACS Appl. Mater. Interfaces 2015, 7, 2444−2451

matrix. The feasibility of this concept has been demonstrated by Feng' works, in which phenol–formaldehyde resol derived carbon and TiO_2 layers were coated on SnO_2/G nanosheets, respectively.[5,25] Nevertheless, toxic precursors or relatively low electrical conductivity of TiO_2 (10^{-5}–10^{-2} S cm^{-1}) may hinder their scalable manufacturing for practical applications to some extent.[29] Therefore, novel SnO_2-based anodes are still highly needed in view of both composite structure design and further practical application in a scalable manner.

Herein, novel sandwich-like structured hybrids are hierarchically assembled, in which SnO_2 NPs are dually fixed and spatially isolated by graphene nanosheets and a Pani coating layer. Specifically, SnO_2 NPs are anchored on reduced graphene oxide nanosheets, and then intimately coated with Pani with the help of phytic acid. Pani is chose as a coating layer due to its flexibility, good conductivity, and easy processing. More importantly, it has been well- accepted that the SEI layer on the conducting polymers surface is relative stable. Therefore, the DF-SnO_2 NPs in the conductive sandwich-like architecture could solve the above-mentioned problems of pure SnO_2 anodes. As a result, the as-prepared DF-SnO_2/G@Pani hybrid electrode exhibits a high capacity of 770 mAh g^{-1}, an excellent rate ability up to 2000 mA g^{-1}, and stable cycle ability for 400 cycles at a current density of 200 mA g^{-1} and 700 times at 1000 mA g^{-1}.

EXPRIMENTAL SECTION

Preparation of Anchored SnO_2 NPs on Graphene Nanosheets (A-SnO_2/G). GO was first synthesized from natural graphite flakes based on the modified Hummers method.[30] A GO aqueous dispersion (3 mg mL^{-1}, 10 mL) and $SnCl_2{\cdot}2H_2O$ (800 mg) were mixed in DI water (200 mL). The mixture was magnetically stirred for 0.5 h at 90 °C. Ammonia was added to adjust the pH value of the dispersion to neutral. After the dispersion was cooled down to room temperature, the resultant precipitate was collected, washed several times with DI water, and dried at 60 °C. To facilitate the following Pani coating, the washed A-SnO_2/G without drying was dispersed in 200 mL DI water, resulting in the uniform A-SnO_2/G suspension. Pure SnO_2 nanoparticles were obtained using the above procedure in the absence of GO according to the following reaction:[5,25]

$$4Sn^{2+}_{(aq)} + 2H_2O + O_{2(g)} \rightarrow 2SnO_{2(s)} + 4H^{+}_{(aq)} \quad (1)$$

Preparation of Dually Fixed SnO_2 NPs on Graphene by Pani Coating (DF-SnO_2/G@Pani). The DF-SnO_2/G@Pani hybrid was synthesized via the following solution processes. First, solution A, which contains 286 mg of ammonium persulfate and 10 mL of H_2O, was added and mixed with solution B containing 100 mL of A-SnO_2/G suspension (mentioned above), 0.458 mL of aniline monomer, and 0.921 mL of phytic acid (PA), then bath sonicated for 2 min, and aged for an hour; during this period, the solution changed color from brown to dark green (Figure S1, Supporting Information), indicating the polymerization of aniline monomer on A-SnO_2/G.

Characterization of the Composites. All samples were characterized by field-emission scanning electron microscopy (SEM, QUANTA 450, 20KV), transmission electron microscopy (TEM, FEI Tecnai G20, 200 kV), X-ray diffraction (XRD, D/Max 2400 diffractometer, Cu Kα, λ = 1.5406 Å), and nitrogen adsorption/desorption (Micromeritics ASAP 2020 instrument). The surface characteristics of the samples were investigated using a Nicolet-20DXB Fourier transform infrared spectrometer (FTIR). The weight ratio of SnO_2 in the composites (A-SnO_2/G and DF-SnO_2/G@Pani) was estimated by thermogravimetric analysis (TGA, TA-Q50).

Electrochemical Measurement. The electrochemical measurements were conducted using CR2026 coin cells with pure lithium foil as the counter and reference electrodes at room temperature. The working electrode consists of a test material, carbon black, and polyvinylidene difluoride (PVDF) in a weight ratio of 8:1:1. The mixture was spread onto a copper foil and dried at 120 °C for 12 h in vacuum. The electrolyte used was 1.0 M LiPF6 in a 50:50 (wt./wt.) mixture of ethylene carbonate (EC) and diethyl carbonate (DEC). The electrodes were assembled into CR2016-type coin cells with pure lithium foil as the counter and reference electrodes at room temperature in a glovebox. The galvanostatic charge/discharge tests were performed on a LAND CT2000 battery tester at different current densities with a cutoff voltage window of 0.01–3.00 V. The calculation of the specific capacity is based on the total mass of the composite. The cyclic voltammograms (CVs) were conducted using a CHI660D electrochemistry workstation between 0.01 and 3.0 V at a scan rate of 0.1 mV s^{-1}. The electrochemical impedance spectroscopy (EIS) measurements were carried out using a CHI660D workstation by applying the AC amplitude of 5 mV over the frequency range of 100 kHz to 0.01 Hz.

RESULTS AND DISCUSSION

Scheme 1 illustrates that the synthesis of DF-SnO_2/G@Pani nanosheets consists of two main steps: (I) $SnCl_2{\cdot}2H_2O$ was first mixed with GO and treated at 90 °C for 30 min. In the reaction system, Sn^{2+} ions were first adsorbed by oxygen-containing functional groups (such as carboxyl, hydroxyl, and epoxyl) on the GO surface via electrostatic interactions. Because of the reducibility of Sn^{2+} ions and the oxidability of GO, Sn^{2+} ions adsorbed on the GO surface would be *in situ* oxidized by GO to give birth to SnO_2 NPs, while the graphene oxide nanosheets were synchronously reduced to reduced graphene oxide (rGO) nanosheets with the corresponding color of the solution changing from brown yellow to black (Figure S1b).[31] After this reaction, there are still many oxygen-containing functional groups left on rGO nanosheets due to the weak reducibility of Sn^{2+} ions; thus, the fresh and ultrasmall SnO_2 NPs with polar surfaces would interact with those functional groups via hydrogen bonding (Scheme 1). Interactions reported in other metal oxide/rGO systems may also exist, such as chemisorption and van der Waals interactions in Ni(OH)$_2$/rGO,[32] and interactions between TiO_2 NPs and rGO via electrons transferring.[33] Most importantly, a high SnO_2 loading of 89 wt % in A-SnO_2/G could be achieved (Figure S2, Supporting Information), which is favorable for subsequently structural construction for lithium storage applications. In order to avoid the formation of unstable SEI on SnO_2 and enhance the electronic conductivity of the hybrid, we took inspiration

Scheme 1. Schematic Illustration of Synthesis Route of DF-SnO_2/G@Pani and Intimate Interactions between Phytic Acid Doped Pani and SnO_2 NPs

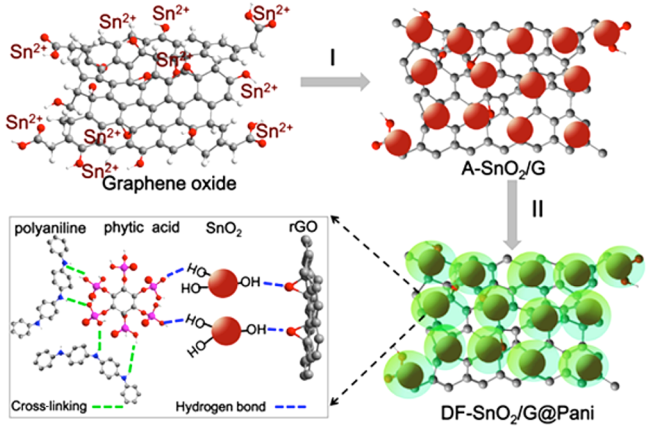

DOI: 10.1021/am506818h
ACS Appl. Mater. Interfaces 2015, 7, 2444–2451

from our daily life, in particular the structure of packaging boxes, in which fragile objects are spatially separated by an elastic sponge and sealed by coverage during transportation; thus, the dually fixed objects would be prevented from mechanical crushing and pollution by impurities. In following step (II), the purified A-SnO_2/G suspension was mixing with phytic acid (PA) and aniline in the presence of ammonium persulfate (APS); after polymerization and cross-linking of aniline on A-SnO_2/G nanosheets (Scheme 1), DF-SnO_2/G@Pani nanosheets could be collected as precipitates. PA plays unique roles in our system: (i) PA works as a dopant to react with the aniline monomer by protonating the nitrogen groups on Pani. (ii) PA serves as a cross-linker to achieve branched Pani during polymerization because each phytic acid molecule can interact with more than one Pani chain, which would benefit the following heterocoating. (iii) The phosphoric acid groups in PA molecules can potentially bind with the SnO_2 surfaces via hydrogen bonding.[34,35] Meanwhile, the negatively charged surface oxide may electrostatically interact with the positively charged Pani doped by PA. All of these roles ensure the subsequent Pani coating on SnO_2 NPs intimately. The content of Pani in the final hybrid could be easily and precisely controlled by adjusting either the amount of input precursor or the polymerization time. Notably, the synthesis of DF-SnO_2/G@Pani here can easily scale up to dozens of grams via our approach (Figure S1).

The morphologies of SnO_2 NPs, A-SnO_2/G, and DF-SnO_2/G@Pani are compared by scanning electron microscopy (SEM) and transmission electron microscopy (TEM). As shown in Figure 1a, A-SnO_2/G inherits the two-dimensional shape of

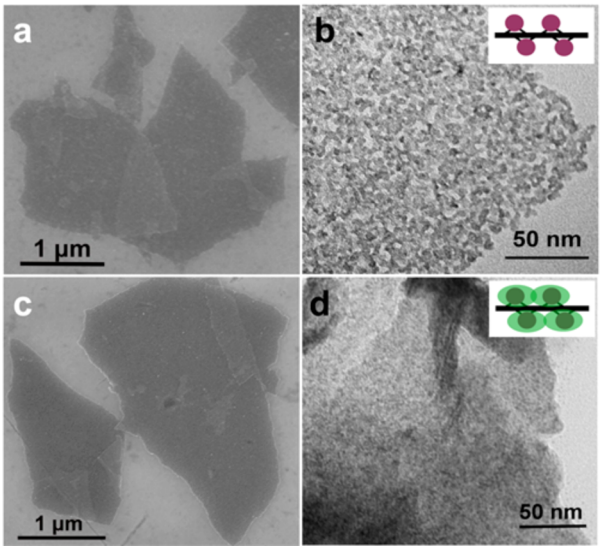

Figure 1. Typical SEM images of mesoporous A-SnO_2/G nanosheets (a) and DF-SnO_2/G@Pani hybrids (c), and TEM images of A-SnO_2/G nanosheets (b) and DF-SnO_2/G@Pani hybrids (d), where the insets schematically show cross-sectional views of the samples.

GO (Figure 1a,b and Figure S3a, Supporting Information), and SnO_2 NPs are uniformly distributed on it. The enlarged photo confirms the presence of mesopores between nanoparticles (Figure 1b). Notably, even after 5 min of ultrasonic treatment, few of NPs fall off from GNs (Figure 1b, Figure S3a), suggesting that SnO_2 NPs are strongly anchored. In contrast, pure SnO_2 nanoparticles tend to severely agglomerate (Figure 1a and Figure S4, Supporting Information). After Pani coating, DF-SnO_2/G@Pani still keeps the 2D morphology of A-SnO_2/G nanosheets, and no free Pani particles could be recognized (Figure 1c,d). Compared with the transparent GNs under the electron irradiation in Figure 1b, an obscure sheet is shown in Figure 1d, indicating the existing of Pani. High-resolution TEM (HRTEM) also reveals that all the inorganic species on the graphene nanosheets have clear lattice fringes; specifically, the marked *d*-spacing with the red arrow in Figure S3c is about 0.33 nm, corresponding to the (110) planes of tetragonal rutile phase SnO_2. Elemental mapping results directly disclose that element Sn corresponding to SnO_2, and element P and N corresponding to PA doped Pani uniformly distribute in the observed zone (Figure 2), strongly suggesting a homogeneous

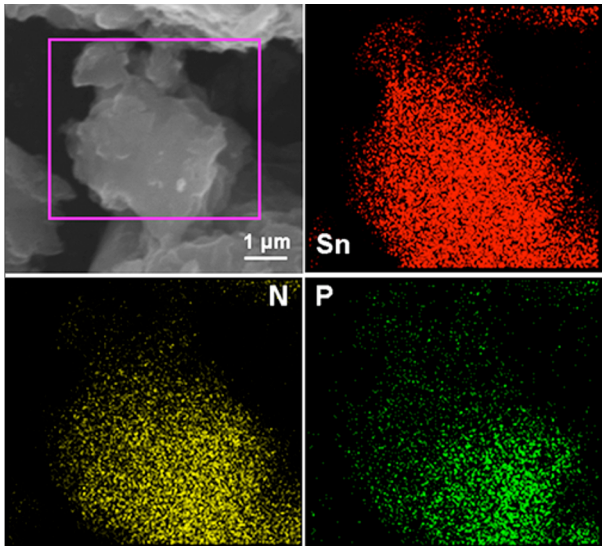

Figure 2. Elemental mapping images of DF-SnO_2/G@Pani hybrid.

Pani coating via the mentioned interactions between PA doped Pani and SnO_2 NPs (Scheme 1). Additionally, the P and N atomic percent in the phytic acid doped Pani is about 4.9% and 9.39% based on elemental analysis (Figure S5, Supporting Information), respectively.

The crystallographic structure and phase purity of the DF-SnO_2/G@Pani hybrid is determined by X-ray powder diffraction (XRD), as shown in Figure 3. The GO exhibit only one peak centered at ca. 11°, corresponding to a basal spacing of ≈0.8 nm. Owing to the introduction of various oxygen-containing functionalities (e.g., carboxyl, hydroxyl, or epoxy) between layers, the basal spacing was greatly expanded

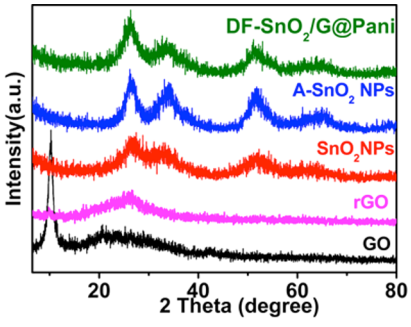

Figure 3. XRD patterns of GO, rGO, SnO_2 NPs, A-SnO_2/G, and DF-SnO_2/G@Pani hybrid.

DOI: 10.1021/am506818h
ACS Appl. Mater. Interfaces 2015, 7, 2444−2451

from 0.335 nm (pristine graphite) to 0.779 nm (GO). Interestingly, in contrast to the broad peak around 26° of the rGO pattern, the graphene-based SnO_2 composites, either A-SnO_2/G or DF-SnO_2/G@Pani, have similar XRD patterns corresponding to the SnO_2 structure without the appearance of the 11° peak for GO, suggesting the transformation of GO into graphene by Sn^{2+} reduction.[31] All the XRD peaks for A-SnO_2/G and DF-SnO_2/G@Pani are indexable to the tetragonal SnO_2 structure (JCPDS 41-1445), indicating the formation of pure SnO_2 crystals. The conventional stacking peak of nanosheets, usually located at ca. 26°, is also absent in the patterns. This implies that the formation of SnO_2 nanoparticles on the surfaces of graphene nanosheets prevents the graphene nanosheets from restacking. There are no obvious pattern changes after Pani coating compared with that of the initial A-SnO_2/G, indicating that the Pani coating just forms on the surface of A-SnO_2/G and does not change the phase of SnO_2.

Nitrogen physisorption measurements were carried out to trace the change of pore structure before and after Pani coating. The Brunauer–Emmett–Teller (BET) surface area for A-SnO_2/G is calculated to be 295 m^2 g^{-1}, and the pore size distribution is centered on 3 nm (Figure 4). Furthermore, the

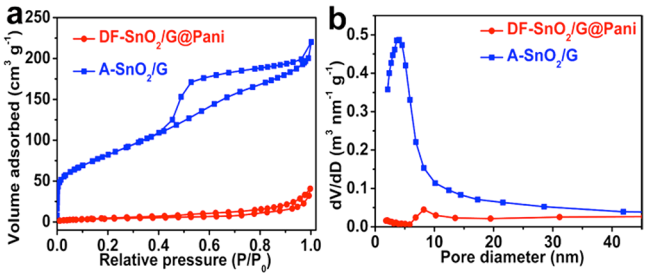

Figure 4. Nitrogen adsorption–desorption isotherms (a) and pore size distribution (b) of the A-SnO_2/G and DF-SnO_2/G@Pani hybrids.

adsorption–desorption isotherm of A-SnO_2/G exhibits the typical type IV nitrogen adsorption branch with an H2 hysteresis loop, indicating the mesoporous structure, which should originate from the interval spaces among SnO_2 NPs based on the above TEM observations. In other words, SnO_2 NPs are anchored and spatially isolated. During the following Pani coating, SnO_2 NPs are fully embedded in the Pani layer, due to the unique roles of PA (Scheme 1),[34−36] as indicated, the low SSA of 15 m^2 g^{-1} with rarely porous structures of DF-SnO_2/G@Pani hybrid (Figure 1d, Scheme 1). Therefore, spatially isolated SnO_2 NPs are dually fixed by the graphene substrate and flexible Pani coating layer, which are applauded for further lithium-ion battery applications.

The variation of surface characteristics from GO to DF-SnO_2/G@Pani are recorded by FTIR measurements. In the spectrum of GO (Figure 5), the absorption peaks at 1723, 1380, 1061, and 1615 cm^{-1} can be ascribed to stretching vibrations of C═O, −OH, epoxy C−O bonds, and C−C aromatic ring modes, respectively.[37] In the spectrum of the A-SnO_2/G sample, the intensity of the peaks from oxygen-containing groups is greatly suppressed due to the removal of oxygen-containing groups, while new apparent peaks arise at 600 cm^{-1}, which could be ascribed to the terminal oxygen vibration (Sn−OH).[31,38] After Pani coating, no apparent peaks related to SnO_2 or graphene signals could be detected, and there are two characteristic peaks located at 1570 and 1480 cm^{-1} corresponding to the stretching vibration of the quinoid

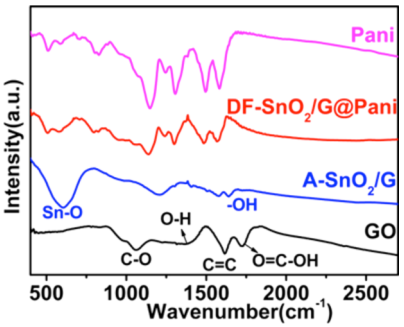

Figure 5. FTIR spectra of GO, SnO_2 NPs, A-SnO_2/G, and DF-SnO_2/G@Pani hybrids.

ring and benzenoid ring,[35] respectively, which indicates the formation of emeraldine salt from PA doped Pani. This information strongly suggests the complete coverage of a Pani shell on A-SnO_2/G and demonstrates our designed route (Scheme 1); thus, the direct contact between SnO_2 and electrolyte can be efficiently avoided when used as electrode materials, preventing the formation of unstable SEI films. Thermogravimetric analysis (TGA) analysis shows the overall contents of SnO_2, Pani, and G in the DF-SnO_2/G@Pani hybrid are ca. 65, 8, and 27 wt % (Figure S2).

The presence of a delicate Pani coating in the DF-SnO_2/G@Pani hybrid is capable of serving as the structural buffering layer to allow the volume variation upon lithium storage reaction and protecting SnO_2 nanoparticles from severe structural degradation. In addition, the ultrasmall SnO_2 nanoparticles also offer several structural advantages to facilitate the lithium storage, including the large surface area, extremely reduced diffusion path, and enhanced channel for electron transport.[1] Motivated by the great potential of conductive polymer-coated nanostructures in LIBs, the electrochemical properties of the DF-SnO_2/G@Pani hybrid are investigated. In general, the electrochemical process of SnO_2-based electrodes can be described by the following principal reactions:

$$SnO_2 + 4Li^+ + 4e^- \rightarrow Sn + 2Li_2O \quad (2)$$

$$Sn + xLi^+ + xe^- \leftrightarrow Li_xSn\ (0 \le x \le 4.4) \quad (3)$$

Figure 6a displays the cyclic voltammetry curves (CVs) for the first 3 cycles, which were obtained between 0.01 and 3.0 V at a scan rate of 0.1 mV s^{-1}. In the first cycle, a pronounced cathodic peak is observed at about 0.8 V that disappears in the subsequent cycles. It can be ascribed to the irreversible reactions during lithium storage reaction such as the formation of solid electrolyte interface (SEI) film and the formation of Li_2O by the reduction of SnO_2 to metallic Sn. The subsequent CV curves show good reproducibility with several cathodic and anodic peak pairs, suggesting a very high degree of reversibility of the multistep conversion that involves the alloying and dealloying process of Li_xSn. Figure 6b shows the representative discharge/charge voltage profiles of the DF-SnO_2/G@Pani hybrid at a current density of 100 mA g^{-1} within a cutoff window of 0.01−3.0 V in the 1st, 2nd, 20th, and 50th cycles; the discharge/charge behaviors are well consistent with CV results. Apparently, the Pani coating does not change the lithium storage behavior of SnO_2. In contrast to the obvious capacity fade in Figure 6c, there is a slight capacity increase, which may be ascribed to the formation of SEI films and

DOI: 10.1021/am506818h
ACS Appl. Mater. Interfaces 2015, 7, 2444−2451

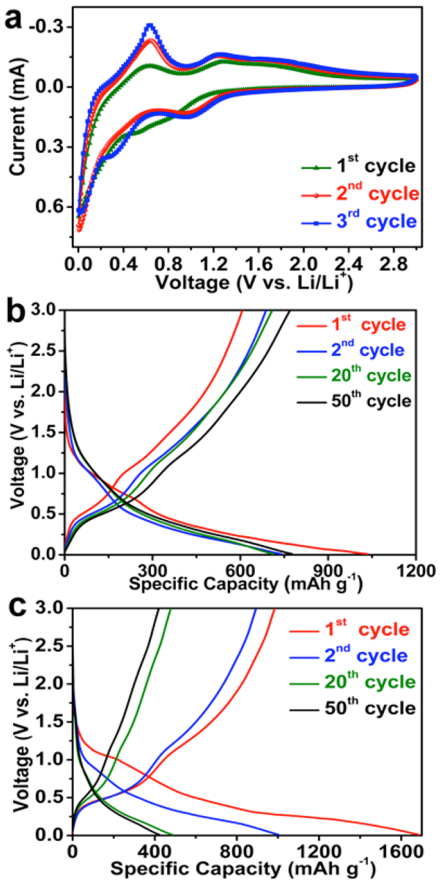

Figure 6. (a) CV curves up to three cycles for the DF-SnO_2/G@Pani hybrid, and discharge/charge profiles of the DF-SnO_2/G@Pani (b) and A-SnO_2/G hybrid (c).

activation of the electrochemical active materials during lithiation.

Figure 7a shows the cycling performance of DF-SnO_2/G@Pani hybrids at a current density of 100 mA g^{-1} within a cutoff window of 0.01−3.0 V. The initial discharge and charge capacities are found to be 1032 and 605 mAh g^{-1}, respectively. The large capacity loss in the first cycle is mainly attributed to the initial irreversible formation of Li_2O, and other irreversible processes such as trapping of some lithium in the lattice, inevitable formation of SEI layer, and electrolyte decomposition, which are common for most anode materials.[39,40] In the initial 25 cycles, it exhibits a capacity of over 710 mAh g^{-1}. From the 26th to 30th cycles, there is a slight capacity rise (about 60 mAh g^{-1}); such a capacity increase is relatively common for nanostructured metal oxide based anodes. One possible reason is the reversible formation of an organic polymeric/gel-like layer due to the electrolyte decomposition to deliver excess capacity through a "pseudocapacitance-type behavior".[2,41,42] Furthermore, the activation of the active materials could also contribute to the capacity rise in metal oxide anodes.[43] From the 30th cycle onward, the DF-SnO_2/G@Pani anode delivers a stable capacity over 100 cycles. For the A-SnO_2/G hybrid and SnO_2 NPs, the capacities decay much faster to less than 400 mAh g^{-1} within 60 cycles. Pani is electrochemically inactive in the voltage window tested and does not contribute to the observed capacity; thus, the appropriate amount of Pani is important to the final electrochemical performance. Too less or more Pani contents may lead to an imperfect coating or excess electrochemical inactive materials in the final hybrids, resulting in inferior electrochemical performance (Figure S6, Supporting Information). Furthermore, the SnO_2/G@Pani anode without PA exhibits poor cycling stability (Figure S7, Supporting Information), demonstrating the unique roles of PA mentioned above. Apparently, the DF-SnO_2/G@Pani hybrid exhibits superior electrochemical performance to that of SnO_2 and A-SnO_2/G hybrid, further indicating our rational design of nanoengineering strategy. Nanostructures electrode in combination with poor crystalline may be responsible for the high capacity[1,24,42,44]

Generally, SnO_2-based anodes are observed to suffer from the disadvantages of sluggish kinetics and poor conductivity; however, the DF-SnO_2/G@Pani hybrid shows excellent cycling response to continuously varying current densities despite this. Even cycled at high current densities of 500−2000 mA g^{-1},

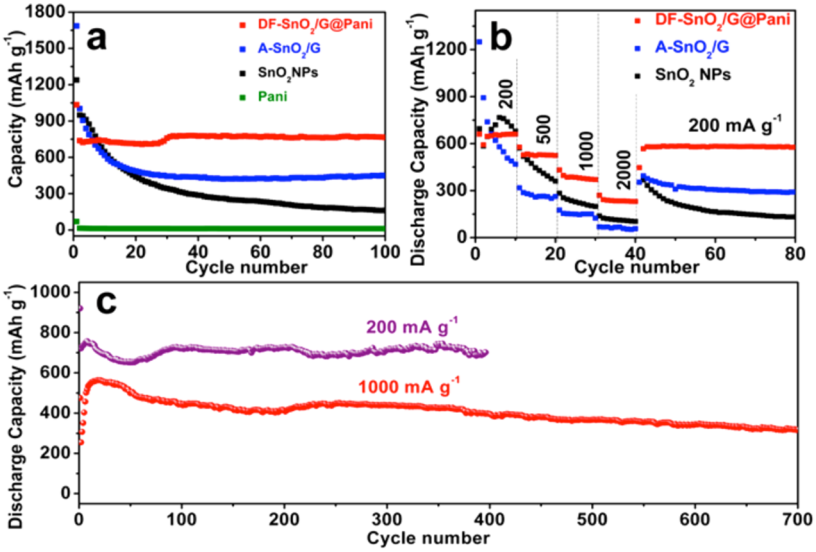

Figure 7. (a) Cycling performance of the pure Pani, SnO_2 NPs, A-SnO_2, and DF-SnO_2/G@Pani electrodes. (b) Rate performance of SnO_2 NPs, A-SnO_2, and DF-SnO_2/G@Pani electrodes. (c) Long life cycling performance of the DF-SnO_2/G@Pani electrode.

DOI: 10.1021/am506818h
ACS Appl. Mater. Interfaces 2015, 7, 2444−2451

comparable capacities of 240−530 mAh g^{-1} can still be maintained, as shown in Figure 7b. After deep cycling at 2000 mA g^{-1}, a stable high capacity could be largely restored for repeated cycles after abruptly switching the current density back to 200 mA g^{-1}, indicating the excellent robustness and stability of the hybrids. As a comparison, the rate performance of DF-SnO_2/G@Pani, A-SnO_2/G hybrid, and SnO_2 NPs is also shown in Figure 7b. These materials exhibit fast capacity fading with current density increasing, and most of the capacities are lost at high current densities of 1000−2000 mA g^{-1}. The long-term cycling tests show that the DF-SnO_2/G@Pani hybrid could exhibit high capacity retention of over 90% for 400 cycles with a high capacity of ca. 700 mAh g^{-1} at a current density of 200 mA g^{-1} (Figure 7c). The TEM image of a cycled electrode suggested that the two-dimensional nanostructure of the DF-SnO_2/G@Pani hybrid kept well without Pani degradation and SnO_2 NPs falling off the nanosheets (Figure S8, Supporting Information), indicating the successful construction of dually fixed SnO_2 NPs via our reasonably designed route. When cycled at a higher current density of 1000 mA g^{-1}, because the active material SnO_2 NPs were sandwiched between Pani and graphene sheets, the utilization of them increases, corresponding to the initial capacity rise with cycles. The hybrid can deliver stable cycling ability with only 0.28 mAh g^{-1} per cycle capacity fading from the 50th to the 700th cycle. Such a remarkable electrochemical performance is superior to most of SnO_2-based anode materials.[16,18,20,45,46]

The superior electrochemical performance of DF-SnO_2/G@Pani should be ascribed to several structural merits. (1) The SnO_2 NPs uniformly anchored on graphene nanosheets and spatially separated by Pani with the help of phytic acid would not cause serious aggregation during repeatedly discharge/charge cycles; meanwhile, the swelling nature of Pani and flexible graphene nanosheets would accommodate SnO_2 NPs volume expansion during lithiation (Scheme 2), keeping the structural integrity of the overall electrode. (2) The 2D sandwich-like structure may ensure the short path for electrolyte and ions; meanwhile, conductive Pani and graphene nanosheets would facilitate electron transport, as evidenced by the drastically reduced diameter of the semicircle of DF-SnO_2/G@Pani at the high-frequency region in the electrochemical impedance spectroscopy (EIS) patterns (Figure S9, Supporting Information). (3) The Pani shell can prevent the encapsulated SnO_2 NPs from directly contacting with the electrolyte and form the unstable SEI films (Scheme 2). Therefore, the lithium storage properties of our DF-SnO_2/G@Pani hybrid are thus remarkably improved.

Scheme 2. Schematic Illustration of the Changes of A-SnO_2/G and DF-SnO_2/G@Pani Electrodes upon Lithiation

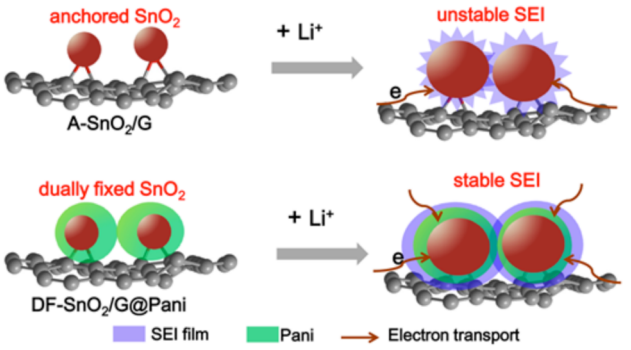

CONCLUSIONS

In summary, we have developed a two-step wet chemistry route to achieve spatially separated and dually fixed SnO_2 nanoparticles by a graphene nanosheet anchoring substrate and a polyaniline coating layer. During the repeated charge/discharge cycles, such a sandwich-like structure would enhance the conductivity of SnO_2 NPs, accommodate the volume variation, and form stable SEI films; therefore, the final DF-SnO_2/G@Pani electrode exhibits high capacity comparative with the theoretical capacity of pure SnO_2, excellent rate ability, and long cycle life up to 700 times. The present nanoengineering strategy can be further extended to build up various 2D core−shell nanomaterials for energy storage and conversion in the low-cost and scale manner.

ASSOCIATED CONTENT

Supporting Information

Photo images of the mixed solution of GO and $SnCl_2 \cdot 2H_2O$, A-SnO_2/G and DF-SnO_2/G@Pani suspension. TEM images of A-SnO_2/G, DF-SnO_2/G@Pani hybrids, and HRTEM image of DF-SnO_2/G@Pani hybrid, elemental analysis of PA doped Pani, cycling stability of DF-SnO_2/G@Pani hybrids with 14.6 and 32.6 wt % Pani content, cycling performance of SnO_2/G@Pani anode without PA, TEM image of cycled DF-SnO_2/G@Pani anode and Nyquist plots of the SnO_2 NPs, A-SnO_2/G and DF-SnO_2/G@Pani electrodes. This material is available free of charge via the Internet at http://pubs.acs.org.

AUTHOR INFORMATION

Corresponding Authors

*E-mail: zbzhao@dlut.edu.cn (Z.Z.).
*E-mail: jqiu@dlut.edu.cn (J.Q.).

Author Contributions

The manuscript was written through contributions of all authors. All authors have given approval to the final version of the manuscript.

Notes

The authors declare no competing financial interest.

ACKNOWLEDGMENTS

This work was supported by the NSFC (No. 51072028).

ABBREVIATIONS

APS, ammonium persulfate
PA, phytic acid
GNs, graphene nanosheets
rGO, reduced graphene oxide
Pani, polyaniline
EIS, electrochemical impedance spectroscopy

REFERENCES

(1) Arico, A. S.; Bruce, P.; Scrosati, B.; Tarascon, J.-M.; van Schalkwijk, W. Nanostructured Materials for Advanced Energy Conversion and Storage Devices. *Nat. Mater.* **2005**, *4*, 366−377.
(2) Wang, Z.; Luan, D.; Madhavi, S.; Hu, Y.; Lou, X. W. Assembling Carbon-Coated α-Fe_2O_3 Hollow Nanohorns on the CNT Backbone for Superior Lithium Storage Capability. *Energy Environ. Sci.* **2012**, *5*, 5252−5256.

DOI: 10.1021/am506818h
ACS Appl. Mater. Interfaces 2015, 7, 2444−2451

(3) Ji, L.; Lin, Z.; Alcoutlabi, M.; Zhang, X. Recent Developments in Nanostructured Anode Materials for Rechargeable Lithium-Ion Batteries. *Energy Environ. Sci.* **2011**, *4*, 2682−2699.
(4) Zhang, L.; Zhang, G.; Wu, H. B.; Yu, L.; Lou, X. W. Hierarchical Tubular Structures Constructed by Carbon-Coated SnO_2 Nanoplates for Highly Reversible Lithium Storage. *Adv. Mater.* **2013**, *25*, 2589−2593.
(5) Tang, Y.; Wu, D.; Chen, S.; Zhang, F.; Jia, J.; Feng, X. Highly Reversible and Ultra-Fast Lithium Storage in Mesoporous Graphene-Based TiO_2/SnO_2 Hybrid Nanosheets. *Energy Environ. Sci.* **2013**, *6*, 2447−2451.
(6) Lin, J.; Peng, Z.; Xiang, C.; Ruan, G.; Yan, Z.; Natelson, D.; Tour, J. M. Graphene Nanoribbon and Nanostructured SnO_2 Composite Anodes for Lithium Ion Batteries. *ACS Nano* **2013**, *7*, 6001−6006.
(7) Huang, J. Y.; Zhong, L.; Wang, C. M.; Sullivan, J. P.; Xu, W.; Zhang, L. Q.; Mao, S. X.; Hudak, N. S.; Liu, X. H.; Subramanian, A.; Fan, H.; Qi, L.; Kushima, A.; Li, J. In Situ Observation of the Electrochemical Lithiation of a Single SnO_2 Nanowire Electrode. *Science* **2010**, *330*, 1515−1520.
(8) Wang, Z.; Luan, D.; Boey, F. Y. C.; Lou, X. W. Fast Formation of SnO_2 Nanoboxes with Enhanced Lithium Storage Capability. *J. Am. Chem. Soc.* **2011**, *133*, 4738−4741.
(9) Wang, C.; Zhou, Y.; Ge, M.; Xu, X.; Zhang, Z.; Jiang, J. Z. Large-Scale Synthesis of SnO_2 Nanosheets with High Lithium Storage Capacity. *J. Am. Chem. Soc.* **2009**, *132*, 46−47.
(10) Wang, Z.; Zhou, L.; Lou, X. W. Metal Oxide Hollow Nanostructures for Lithium-Ion Batteries. *Adv. Mater.* **2012**, *24*, 1903−1911.
(11) Ding, L.; He, S.; Miao, S.; Jorgensen, M. R.; Leubner, S.; Yan, C.; Hickey, S. G.; Eychmüller, A.; Xu, J.; Schmidt, O. G. Ultrasmall SnO_2 Nanocrystals: Hot-Bubbling Synthesis, Encapsulation in Carbon Layers and Applications in High Capacity Li-Ion Storage. *Sci. Rep.* **2014**, *4*, 4647−4654.
(12) Li, D.; Qin, Q.; Duan, X.; Yang, J.; Guo, W.; Zheng, W. General One-Pot Template-Free Hydrothermal Method to Metal Oxide Hollow Spheres and Their Photocatalytic Activities and Lithium Storage Properties. *ACS Appl. Mater. Interfaces* **2013**, *5*, 9095−9100.
(13) Ye, J.; Zhang, H.; Yang, R.; Li, X.; Qi, L. Morphology-Controlled Synthesis of SnO_2 Nanotubes by Using 1D Silica Mesostructures as Sacrificial Templates and Their Applications in Lithium-Ion Batteries. *Small* **2010**, *6*, 296−306.
(14) Chen, J. S.; Lou, X. W. SnO_2 and TiO_2 Nanosheets for Lithium-Ion Batteries. *Mater. Today* **2012**, *15*, 246−254.
(15) Wang, X.; Cao, X.; Bourgeois, L.; Guan, H.; Chen, S.; Zhong, Y.; Tang, D.-M.; Li, H.; Zhai, T.; Li, L.; Bando, Y.; Golberg, D. N-Doped Graphene-SnO_2 Sandwich Paper for High-Performance Lithium-Ion Batteries. *Adv. Funct. Mater.* **2012**, *22*, 2682−2690.
(16) Yang, S.; Yue, W.; Zhu, J.; Ren, Y.; Yang, X. Graphene-Based Mesoporous SnO_2 with Enhanced Electrochemical Performance for Lithium-Ion Batteries. *Adv. Funct. Mater.* **2013**, *23*, 3570−3576.
(17) Xu, C.; Sun, J.; Gao, L. Direct Growth of Monodisperse SnO_2 Nanorods on Graphene as High Capacity Anode Materials for Lithium Ion Batteries. *J. Mater. Chem.* **2012**, *22*, 975−979.
(18) Huang, Y.; Wu, D.; Han, S.; Li, S.; Xiao, L.; Zhang, F.; Feng, X. Assembly of Tin Oxide/Graphene Nanosheets into 3D Hierarchical Frameworks for High-Performance Lithium Storage. *ChemSusChem* **2013**, *6*, 1510−1515.
(19) Zhou, X.; Wan, L.-J.; Guo, Y.-G. Binding SnO_2 Nanocrystals in Nitrogen-Doped Graphene Sheets as Anode Materials for Lithium-Ion Batteries. *Adv. Mater.* **2013**, *25*, 2152−2157.
(20) Wang, X.; Zhou, X.; Yao, K.; Zhang, J.; Liu, Z. A SnO_2/Graphene Composite as a High Stability Electrode for Lithium Ion Batteries. *Carbon* **2011**, *49*, 133−139.
(21) Wang, R.; Xu, C.; Sun, J.; Gao, L.; Yao, H. Solvothermal-Induced 3D Macroscopic SnO_2/Nitrogen-Doped Graphene Aerogels for High Capacity and Long-Life Lithium Storage. *ACS Appl. Mater. Interfaces* **2014**, *6*, 3427−3436.
(22) Liang, J.; Wei, W.; Zhong, D.; Yang, Q.; Li, L.; Guo, L. One-Step In Situ Synthesis of SnO_2/Graphene Nanocomposites and Its Application as an Anode Material for Li-Ion Batteries. *ACS Appl. Mater. Interfaces* **2011**, *4*, 454−459.
(23) Ding, S.; Luan, D.; Boey, F. Y. C.; Chen, J. S.; Lou, X. W. SnO_2 Nanosheets Grown on Graphene Sheets with Enhanced Lithium Storage Properties. *Chem. Commun.* **2011**, *47*, 7155−7157.
(24) Wang, Z.; Wang, Z.; Liu, W.; Xiao, W.; Lou, X. W. Amorphous $CoSnO_3$@C Nanoboxes with Superior Lithium Storage Capability. *Energy Environ. Sci.* **2013**, *6*, 87−91.
(25) Su, Y.; Li, S.; Wu, D.; Zhang, F.; Liang, H.; Gao, P.; Cheng, C.; Feng, X. Two-Dimensional Carbon-Coated Graphene/Metal Oxide Hybrids for Enhanced Lithium Storage. *ACS Nano* **2012**, *6*, 8349−8356.
(26) Zhang, B.; Yu, X.; Ge, C.; Dong, X.; Fang, Y.; Li, Z.; Wang, H. Novel 3-D Superstructures Made up of SnO_2@C Core-Shell Nanochains for Energy Storage Applications. *Chem. Commun.* **2010**, *46*, 9188−9190.
(27) Yesibolati, N.; Shahid, M.; Chen, W.; Hedhili, M. N.; Reuter, M. C.; Ross, F. M.; Alshareef, H. N. SnO_2 Anode Surface Passivation by Atomic Layer Deposited HfO_2 Improves Li-Ion Battery Performance. *Small* **2014**, *10*, 2849−2858.
(28) Guan, C.; Wang, X.; Zhang, Q.; Fan, Z.; Zhang, H.; Fan, H. J. Highly Stable and Reversible Lithium Storage in SnO_2 Nanowires Surface Coated with a Uniform Hollow Shell by Atomic Layer Deposition. *Nano Lett.* **2014**, *14*, 4852−4858.
(29) Lu, X.; Yu, M.; Wang, G.; Zhai, T.; Xie, S.; Ling, Y.; Tong, Y.; Li, Y. H-TiO_2@MnO_2//H-TiO_2@C Core−Shell Nanowires for High Performance and Flexible Asymmetric Supercapacitors. *Adv. Mater.* **2013**, *25*, 267−272.
(30) Hu, H.; Zhao, Z.; Zhou, Q.; Gogotsi, Y.; Qiu, J. The Role of Microwave Absorption on Formation of Graphene from Graphite Oxide. *Carbon* **2012**, *50*, 3267−3273.
(31) Li, Y.; Lv, X.; Lu, J.; Li, J. Preparation of SnO_2-Nanocrystal/Graphene-Nanosheets Composites and Their Lithium Storage Ability. *J. Phys. Chem. C* **2010**, *114*, 21770−21774.
(32) Wang, H.; Robinson, J. T.; Diankov, G.; Dai, H. Nanocrystal Growth on Graphene with Various Degrees of Oxidation. *J. Am. Chem. Soc.* **2010**, *132* (10), 3270−3271.
(33) Kamat, P. V. Graphene-Based Nanoarchitectures. Anchoring Semiconductor and Metal Nanoparticles on a Two-Dimensional Carbon Support. *J. Phys. Chem. Lett.* **2009**, *1* (2), 520−527.
(34) Wu, H.; Yu, G.; Pan, L.; Liu, N.; McDowell, M. T.; Bao, Z.; Cui, Y. Stable Li-Ion Battery Anodes by in-Situ Polymerization of Conducting Hydrogel to Conformally Coat Silicon Nanoparticles. *Nat. Commun.* **2013**, *4*, 1943−1948.
(35) Pan, L.; Yu, G.; Zhai, D.; Lee, H. R.; Zhao, W.; Liu, N.; Wang, H.; Tee, B. C.-K.; Shi, Y.; Cui, Y.; Bao, Z. Hierarchical Nanostructured Conducting Polymer Hydrogel with High Electrochemical Activity. *Proc. Natl. Acad. Sci. U.S.A.* **2012**, *109*, 9287−9292.
(36) Liu, B.; Soares, P.; Checkles, C.; Zhao, Y.; Yu, G. Three-Dimensional Hierarchical Ternary Nanostructures for High-Performance Li-Ion Battery Anodes. *Nano Lett.* **2013**, *13*, 3414−3419.
(37) Park, S.; Lee, K.-S.; Bozoklu, G.; Cai, W.; Nguyen, S. T.; Ruoff, R. S. Graphene Oxide Papers Modified by Divalent Ions—Enhancing Mechanical Properties via Chemical Cross-Linking. *ACS Nano* **2008**, *2*, 572−578.
(38) Sun, Y.; Lei, F.; Gao, S.; Pan, B.; Zhou, J.; Xie, Y. Atomically Thin Tin Dioxide Sheets for Efficient Catalytic Oxidation of Carbon Monoxide. *Angew. Chem., Int. Ed.* **2013**, *52*, 10569−10572.
(39) Liang, J.; Cai, Z.; Tian, Y.; Li, L.; Geng, J.; Guo, L. Deposition SnO_2/Nitrogen-Doped Graphene Nanocomposites on the Separator: A New Type of Flexible Electrode for Energy Storage Devices. *ACS Appl. Mater. Interfaces* **2013**, *5*, 12148−12155.
(40) Zhou, Q.; Zhao, Z.; Wang, Z.; Dong, Y.; Wang, X.; Gogotsi, Y.; Qiu, J. Low Temperature Plasma Synthesis of Mesoporous Fe_3O_4 Nanorods Grafted on Reduced Graphene Oxide for High Performance Lithium Storage. *Nanoscale* **2014**, *6*, 2286−2291.
(41) Laruelle, S.; Grugeon, S.; Poizot, P.; Dollé, M.; Dupont, L.; Tarascon, J. M. On the Origin of the Extra Electrochemical Capacity

DOI: 10.1021/am506818h
ACS Appl. Mater. Interfaces 2015, 7, 2444−2451

Displayed by MO/Li Cells at Low Potential. *J. Electrochem. Soc.* **2002**, *149*, A627−A634.
(42) Poizot, P.; Laruelle, S.; Grugeon, S.; Dupont, L.; Tarascon, J. M. Nano-Sized Transition-Metal Oxides as Negative-Electrode Materials for Lithium-Ion Batteries. *Nature* **2000**, *407*, 496−499.
(43) Sun, H.; Xin, G.; Hu, T.; Yu, M.; Shao, D.; Sun, X.; Lian, J. High-Rate Lithiation-Induced Reactivation of Mesoporous Hollow Spheres for Long-Lived Lithium-Ion Batteries. *Nat. Commun.* **2014**, *5*, 1038−1045.
(44) Shin, J.-Y.; Joo, J. H.; Samuelis, D.; Maier, J. Oxygen-Deficient $TiO_{2-\delta}$ Nanoparticles via Hydrogen Reduction for High Rate Capability Lithium Batteries. *Chem. Mater.* **2011**, *24*, 543−551.
(45) Liang, R.; Cao, H.; Qian, D.; Zhang, J.; Qu, M. Designed Synthesis of SnO_2-Polyaniline-Reduced Graphene Oxide Nanocomposites as an Anode Material for Lithium-Ion Batteries. *J. Mater. Chem.* **2011**, *21*, 17654−17657.
(46) Liang, J.; Zhao, Y.; Guo, L.; Li, L. Flexible Free-Standing Graphene/SnO_2 Nanocomposites Paper for Li-Ion Battery. *ACS Appl. Mater. Interfaces* **2012**, *4*, 5742−5748.

DOI: 10.1021/am506818h
ACS Appl. Mater. Interfaces 2015, 7, 2444−2451